One-dimensional laser cooling with linearly polarized fields

Jun Guo* and Paul R. Berman†
Physics Department, New York University, 4 Washington Place, New York, New York 10003
(Received 26 April 1993)

We present a calculation of one-dimensional sub-Doppler cooling of neutral atoms, in which the atomic center-of-mass motion is quantized. The cooling field consists of a pair of counterpropagating, linearly polarized laser beams, with their polarizaton vectors at an angle θ with respect to each other. The steady-state atomic density matrix is analyzed as a function of θ. It is shown that, depending on the internal atomic level scheme, the equilibrium population of the quantized ground state of atomic center-of-mass motion can either increase or decrease significantly when θ is reduced from $\pi/2$. These effects are interpreted based on the spatial localization of atoms in the light-induced potential wells.

PACS number(s): 32.80.Pj, 42.50.Vk

I. INTRODUCTION

Recently, there has been considerable progress in understanding the physical mechanisms which contribute to sub-Doppler laser cooling of neutral atoms. In the one-dimensional (1D) case, some novel experiments have revealed that, in the usual Sisyphus cooling scheme, where the cooling field consists of a pair of linearly polarized laser beams with their polarization vectors orthogonal (lin⊥lin), quantization of the center-of-mass motion of the atoms is necessary to correctly describe the atomic motion in the optical potentials produced by the radiation fields. Evidence for quantized states of atomic motion is provided by the motional sidebands seen in the pump-probe absorption or fluorescence spectra of atoms [1,2]. A similar situation is also found in the magnetically induced laser-cooling configuration, where the polarization gradient of the laser field is replaced by the addition of a transverse magnetic field [3]. Under these circumstances, the usual approaches for calculating the equilibrium atomic density matrix based on the calculations of frictional forces on free atoms and steady-state atomic momentum diffusion coefficients are no longer considered to be appropriate [4]. One needs to quantize the atomic center-of-mass motion in order to take into account the spatial localization effects.

Several approaches have been developed so far to include the quantized motion of atoms in the Sisyphus cooling scheme. One can discretize the atomic center-of-mass momentum, for example, and obtain a set of generalized optical Bloch equations (GOBE) for the atomic density-matrix elements [5]. By integrating these equations numerically, one can solve for the transient or equilibrium atomic distribution functions in momentum or position spaces. A different approach is based on the Monte Carlo simulation of the atomic wave-function evolutions in the cooling fields [6,7]. Theoretical results based on these approaches show that, for laser intensities somewhat above those required for achieving optimal sub-Doppler cooling, the equilibrium atomic distribution functions are modulated in space. The peaks of the spatial population distribution coincide with the minima of the light-induced potentials, indicating that the cooled atoms are partially localized inside the periodic potential wells.

In this paper, we investigate the case of 1D Sisyphus cooling with a pair of counterpropagating, linearly polarized laser fields, whose polarization vectors are at an angle θ with respect to each other (lin∠lin). An earlier calculation for this cooling-field configuration interacting with atoms having ground-state angular momentum $J_g=\frac{1}{2}$ was based on a Fokker-Planck equation [8], in which the atomic population modulation in space was neglected. A somewhat surprising result of that semiclassical calculation was that, at a given light intensity, the minimum value of the average atomic kinetic energy $\langle p^2\rangle/2m$ was not necessarily achieved for $\theta=\pi/2$. Although the absolute minimum value of $\langle p^2\rangle/2m$, obtained for some optimal field intensity, occurs for $\theta=\pi/2$, at laser intensities slightly higher than those for achieving this, the value of $\langle p^2\rangle/2m$ actually decreases with the decrease of θ (see Fig. 8 of Ref. [8]). For different atomic excited-state angular momenta ($J_e=\frac{1}{2}$ or $\frac{3}{2}$), the results are quite similar, and differ only by some scaling factor. In light of the recent experimental observations of the quantized motion of atoms in the lin⊥lin configuration, one can raise the questions of whether or not this particular feature of the mean atomic kinetic energy for $\theta<\pi/2$ holds when the atomic localization effects are taken into account, and if not, how the localization effects affect the equilibrium atomic density matrix. We intend to address these questions in this paper.

The approach adopted in the present calculation is similar to that developed by Castin and Dalibard [9] for the investigation of Sisyphus cooling in the lin⊥lin field configuration. It is based on the expansion of the atomic density matrix in the energy eigenstate basis of atoms moving in the periodic light-shift potentials. This approach has the advantage in that it offers some physical insight into this system, and the atomic density-matrix elements in the energy basis have close relations with some experimentally observable quantities [1,2].

This paper is organized as follows: In Sec. II, we derive the eigenstate energies and wave functions of the atoms moving in the light-induced potentials. Then in Sec. III, the atomic density matrix is expanded in the

eigenstate basis. Using a secular approximation to be defined below, we solve the density-matrix equations to obtain the equilibrium atomic population distribution of the various energy eigenstates and the mean atomic kinetic energy as a function of θ. In Sec. IV, an interpretation of the results is given. We conclude by offering some discussion on the possibilities of experimentally observing the features of the atomic distribution functions predicted by this theory.

II. EIGENSTATES OF ATOMS MOVING IN THE LIGHT-INDUCED POTENTIALS

The polarization vectors of the two incident fields, which are propagating along the z axis, are at angles $\pm\theta/2$ with respect to the x axis. In terms of the spherical components $\epsilon_\pm$ defined by

$$\epsilon_\pm = \mp\frac{1}{\sqrt{2}}(\hat{\mathbf{x}}\pm i\hat{\mathbf{y}}) ,$$

where $\hat{\mathbf{x}}$ and $\hat{\mathbf{y}}$ are unit vectors in the x and y directions, the total field is written as

$$\mathbf{E} = -\frac{1}{\sqrt{2}}E_0\cos\left[kz-\frac{\theta}{2}\right]e^{-i\omega t}\epsilon_+ + \frac{1}{\sqrt{2}}E_0\cos\left[kz+\frac{\theta}{2}\right]e^{-i\omega t}\epsilon_- + \text{c.c.} \tag{1}$$

The atoms are assumed to have ground-state angular momentum $J_g=\frac{1}{2}$ and excited-state angular momentum $J_e=\frac{1}{2}$ or $\frac{3}{2}$. The resonance frequency is ω_0.

We now define a weak-field limit as

$$\chi \ll |\Delta|, \Gamma , \tag{2}$$

where Γ is the excited-state decay rate,

$$\chi = \frac{er_{eg}E_0}{\sqrt{6}\hbar} , \qquad \Delta = \omega-\omega_0 , \tag{3}$$

and er_{eg} is a reduced matrix element of the atomic dipole moment operator. In the weak-field limit, the atomic excited-state quantities can be adiabatically eliminated, and the resulting effective atomic density-matrix equation can be written as [9]

$$\dot{\rho} = \frac{[H_0,\rho]}{i\hbar} + [\dot{\rho}]_{\text{relax}} , \tag{4}$$

where the Hamiltonian H_0 is given by

$$H_0 = \frac{p^2}{2m} + U_+(z)|+\rangle\langle+| + U_-(z)|-\rangle\langle-| . \tag{5}$$

In Eq. (5), $|\pm\rangle$ denote the two ground-state sublevels $|g,\pm\frac{1}{2}\rangle$ and $U_\pm(z)$ are the space-dependent energy shifts of these two sublevels induced by the cooling field. For $J_e=\frac{1}{2}$, these light-shift potentials are given by

$$U_\pm(z) = U_0\cos^2\left[kz\pm\frac{\theta}{2}\right] , \tag{6}$$

while for $J_e=\frac{3}{2}$,

$$U_\pm(z) = U_0\left[\cos^2\left[kz\mp\frac{\theta}{2}\right]+\tfrac{1}{3}\cos^2\left[kz\pm\frac{\theta}{2}\right]\right] , \tag{7}$$

where the quantity U_0 is defined as

$$U_0 = \frac{\hbar\Delta|\chi|^2}{\gamma^2+\Delta^2} . \tag{8}$$

The distance between the potential minima (or maxima) of $U_+(z)$ and $U_-(z)$ is equal to θ/k in the case of $J_e=\frac{1}{2}$, and equal to $\tan^{-1}[\tan(\theta)/2]/k$ in the case of $J_e=\frac{3}{2}$.

The term $[\dot{\rho}]_{\text{relax}}$ in Eq. (4) denotes the contribution of the relaxation processes to the density-matrix evolution. It can be written as

$$[\dot{\rho}]_{\text{relax}} = -\frac{\gamma_0}{2}[A\rho+\rho A] + \gamma_0\int_{-\hbar k}^{\hbar k}dp'\sum_{m=\pm,0}N_m(p')B_m^+e^{-ip'z/\hbar} \times\rho e^{ip'z/\hbar}B_m , \tag{9}$$

where $\gamma_0=\Gamma|\chi|^2/(\gamma^2+\Delta^2)$, and, for $J_e=\frac{1}{2}$,

$$A = \cos^2\left[kz-\frac{\theta}{2}\right]|-\rangle\langle-| + \cos^2\left[kz+\frac{\theta}{2}\right]|+\rangle\langle+| ,$$
$$B_\pm = \sqrt{\tfrac{2}{3}}\cos\left[kz\mp\frac{\theta}{2}\right]|\mp\rangle\langle\mp| , \tag{10}$$
$$B_0 = \frac{1}{\sqrt{3}}\cos\left[kz+\frac{\theta}{2}\right]|+\rangle\langle-| + \frac{1}{\sqrt{3}}\cos\left[kz-\frac{\theta}{2}\right]|-\rangle\langle+| ,$$

while for $J_e=\frac{3}{2}$,

$$A = \left[\cos^2\left[kz+\frac{\theta}{2}\right]+\tfrac{1}{3}\cos^2\left[kz-\frac{\theta}{2}\right]\right]|-\rangle\langle-| + \left[\cos^2\left[kz-\frac{\theta}{2}\right]+\tfrac{1}{3}\cos\left[kz+\frac{\theta}{2}\right]\right]|+\rangle\langle+| ,$$
$$B_\pm = \cos\left[kz\mp\frac{\theta}{2}\right][|\pm\rangle\langle\pm|+\tfrac{1}{3}|\mp\rangle\langle\mp|] , \tag{11}$$
$$B_0 = \frac{\sqrt{2}}{3}\left[\cos\left[kz+\frac{\theta}{2}\right]|+\rangle\langle-| + \cos\left[kz-\frac{\theta}{2}\right]|-\rangle\langle+|\right] .$$

The functions $N_m(p')$ for $m=\pm,0$ in Eq. (9) are the spontaneous photon momentum distribution functions

associated with the σ and π transitions. They are given by [10]

$$N_{\pm}(p')=\frac{3}{8k}\left[1+\frac{p'^2}{k^2}\right],$$
$$N_0(p')=\frac{3}{4k}\left[1-\frac{p'^2}{k^2}\right]. \quad (12)$$

The Hamiltonian H_0 describes the motion of an atom in the level-dependent periodic potentials $U_{\pm}(z)$, whose periodicity is $\lambda/2$. According to Bloch's theorem, the eigenfunctions of atoms moving in these potentials can be expanded in terms of plane-wave states as [11]

$$|\nu,q,\pm\rangle=\sum_{n=-N}^{N} C_{n,\nu}^{(\pm)}(q)|q,2n\rangle , \quad (13)$$

where $\nu=0,1,\ldots,2N$ is the band index, $q\in[-k,k)$ is the Bloch index, $\pm$ denotes the two internal sublevels $|g,\pm\frac{1}{2}\rangle$, and $|q,2n\rangle$ represents a plane-wave state of momentum $2n\hbar k+\hbar q$. The eigenenergies $E_\nu(q)$ and eigenvectors $C_{n,\nu}^{(\pm)}(q)$ can be solved from the Schrödinger equation with the Hamiltonian H_0. For example, in the case of $J_e=\frac{1}{2}$, the energy spectrum and eigenfunctions can be obtained by solving the following linear equations:

$$\left[\left[\frac{\hbar^2(2nk+q)^2}{2m}+\frac{U_0}{2}\right]-E_\nu(q)\right]C_{n,\nu}^{(\pm)}(q)$$
$$+\frac{U_0}{4}[e^{\mp i\theta}C_{n+1,\nu}^{(\pm)}(q)=E^{\pm i\theta}C_{n-1,\nu}^{(\pm)}(q)]=0 ,$$
$$n=-N,\ldots,N . \quad (14)$$

The value of N, chosen such that $C_{\pm N,\nu}^{(\pm)}(q)\approx 0$, depends on the value of U_0/E_k where $E_k=\hbar^2k^2/2m$ is the recoil energy. For the laser intensity range considered in this paper, $N=30$, which corresponds to a plane-wave expansion of the atomic wave functions up to a momentum of order of $60\hbar k$, is usually sufficient.

Since the light-induced potentials, which are functions of $\cos^2(kz\pm\theta/2)$, can be approximated by simple harmonic potentials near the minima of the potential wells, one expects that the deeply bound eigenstates should resemble those of linear harmonic oscillators. This is indeed the case. Figure 1 shows the atomic energy spectrum $E_\nu(q)$, $\nu=0,\ldots,9$, in the first Brillouin zone for the case of $J_e=\frac{1}{2}$. The potential height is given by $U_0/E_k=100$. For this value of U_0/E_k, there are six bands corresponding to bound states ($E_\nu<U_0$, $\nu=0,\ldots,5$). As one can see, the lowest bound-state energies are nearly equally spaced, and are approximately given by $E_\nu=(\nu+\frac{1}{2})\hbar\Omega_{\rm osc}$, where the oscillation frequency $\Omega_{\rm osc}$, is given by

$$\hbar\Omega_{\rm osc}=\hbar\sqrt{2U_0k^2/m}=2\sqrt{U_0/E_k}E_k . \quad (15)$$

The widths of these bands are extremely narrow (the lowest band has a width less than $10^{-4}E_k$), indicating that the tunneling effects for the atoms in the lowest bands are negligible. As one goes to higher-order bands, the energy curves start to resemble those of free particles ($E=p^2/2m$), and the gaps between adjacent bands at $q=0$ or $\pm k$ become extremely small.

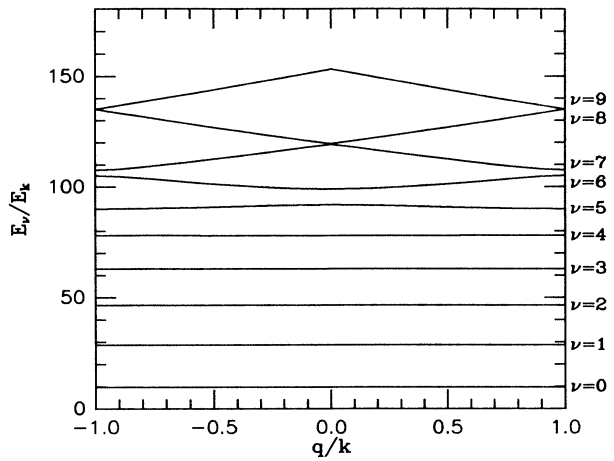

FIG. 1. Energy spectrum of atoms in the first Brillouin zone ($|q|\le k$) when $J_e=\frac{1}{2}$. The potential height is given by $U_0/E_\kappa=100$. The energies of the first 10 bands ($\nu=0,\ldots,9$) are shown. Note that the energy gaps at $q=0$ or $\pm k$ between the highest bands shown are too small to be visible.

III. CALCULATION OF THE EQUILIBRIUM ATOMIC DENSITY MATRIX

After obtaining the eigenstate wave functions of the atoms interacting with the cooling field, one can expand the atomic density matrix in this new eigenstate basis. In general, the density-matrix elements can be written as

$$\rho_{\nu,q,\epsilon;\nu',q',\epsilon'}=\langle\nu,q,\epsilon|\rho|\nu',q',\epsilon'\rangle , \quad (16)$$

where $\epsilon,\epsilon'=\pm$. One then obtains the equations for $\dot\rho_{\nu,q,\epsilon;\nu',q',\epsilon'}$ from Liouville's equation. In order to have a finite number of density-matrix equations, one can impose a periodic boundary condition for the atomic wave functions in a box of some finite length $l(\lambda/2)$, where l is an integer. This leads to a discretization of the Bloch index q, with a discretization interval given by $2k/l$. For the purpose of the present calculation, we choose four index numbers,

$$q=-k,-\frac{k}{2},0,\frac{k}{2} ,$$

corresponding to a normalization length 2λ, which proved to be sufficient. Note that in order to be compatible with this choice of the Bloch index q, one should discretize the spontaneous photon momentum p' in Eq. (9) on the same interval as q.

We now invoke a secular approximation [9] in an effort to simplify the calculation. This approximation assumes that the energy separations between different bands are much greater than the effective widths of various bands due to optical pumping and tunneling effects. If one approximates the potentials $U_{\pm}(z)$ at the minima by a harmonic potential, then this secular approximation can be

written as

$$\gamma_0 \ll \Omega_{\rm ocs} , \tag{17}$$

provided that the populations in the highly excited energy bands are negligible. Inequality (17) is satisfied when $|\Delta| \gg \Gamma$. As a result of the secular approximation, one can neglect the off-diagonal elements between different bands, since they are oscillating at rates much faster than the system relaxation rate γ_0. Furthermore, from Eqs. (9)–(11), one notices that there is no coupling between the off-diagonal elements $\rho_{\nu,q,\epsilon;\nu,q',\epsilon'}$ $(q \neq q',\ \epsilon \neq \epsilon')$ and the diagonal elements $\rho_{\nu,q,\epsilon;\nu,q,\epsilon}$. As a result, under the secular approximation, the only nonvanishing density-matrix elements are the populations of various eigenstates,

$$\pi_{\nu,q,\epsilon} \equiv \rho_{\nu,q,\epsilon;\nu,q,\epsilon} , \tag{18}$$

and one obtains the evolution equations of these elements due to relaxation processes as

$$\dot{\pi}_{\nu,q,\epsilon} = -\gamma_{\nu,q,\epsilon}\pi_{\nu,q,\epsilon} + \sum_{\nu',q',\epsilon'} \gamma(\nu',q',\epsilon' \rightarrow \nu,q,\epsilon)\pi_{\nu',q',\epsilon'} , \tag{19}$$

where

$$\begin{aligned} &\gamma_{\nu,q,\epsilon} = \gamma_0 \langle \nu,q,\epsilon | A | \nu,q,\epsilon \rangle , \\ &\gamma(\nu',q',\epsilon' \rightarrow \nu,q,\epsilon) = \gamma_0 \int_{-\hbar k}^{\hbar k} dp' \sum_m N_m(p') |\langle \nu',q',\epsilon' | e^{ip'z/\hbar} B_m | \nu,q,\epsilon \rangle|^2 , \end{aligned} \tag{20}$$

and A and B_m are given in Eqs. (10) and (11). Introducing a closure relation $1 = \sum_{\nu,q,\epsilon} |\nu,q,\epsilon\rangle\langle\nu,q,\epsilon|$, it is easy to verify, from Eqs. (10), (11), and (20), that the relation $\gamma_{\nu,q,\epsilon} = \sum_{\nu',q',\epsilon'} \gamma(\nu,q,\epsilon \rightarrow \nu',q',\epsilon')$, is satisfied, which is required by population conservation:

$$\sum_{\nu,q,\epsilon} \pi_{\nu,q,\epsilon} = 1 . \tag{21}$$

Equation (19) can be integrated to obtain the solutions for $\pi_{\nu,q,\epsilon}$. However, if one is interested only in the steady-state results, as we are here, a much more efficient way is to set the time derivatives in Eq. (19) to zero and solve the linear equations under the normalization condition Eq. (21). In following this procedure, one first calculates various coefficients $\gamma_{\nu,q,\epsilon}$ and $\gamma(\nu',q',\epsilon' \rightarrow \nu,q,\epsilon)$ from Eq. (20). Some properties of these coefficients are worth noting. First, it is evident from Eqs. (10), (11), and (20) that the detailed balance condition

$$\gamma(\nu',q',\epsilon \rightarrow \nu,q,\epsilon) = \gamma(\nu,q,\epsilon \rightarrow \nu',q',\epsilon) \tag{22}$$

is satisfied. This implies that transitions within an internal sublevel tend to equalize the populations among different bands. They represent a heating mechanism that eventually limits the equilibrium temperature of atoms. On the other hand, one also finds through calculation that

$$\gamma(\nu',q',\pm \rightarrow \nu,q,\mp) > \gamma(\nu,q,\mp \rightarrow \nu',q',\pm) \tag{23}$$

for $\nu' > \nu$. Consequently, transitions between different internal ground-state sublevels tend to accumulate the atomic population in the lowest energy bands, which represent a cooling mechanism (Sisyphus cooling).

After one has obtained the transition probabilities, the equilibrium populations of various bands can be calculat-

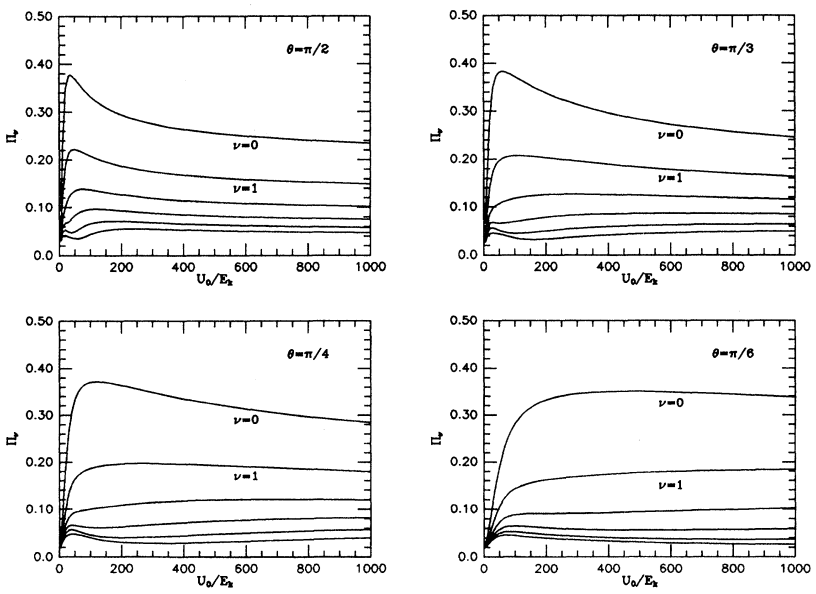

FIG. 2. Atomic populations in the lowest six motional bands as functions U_0/E_k when $J_e = \frac{1}{2}$. For all cases, the band population decreases as the band index increases ($\nu = 0, \ldots, 5$).

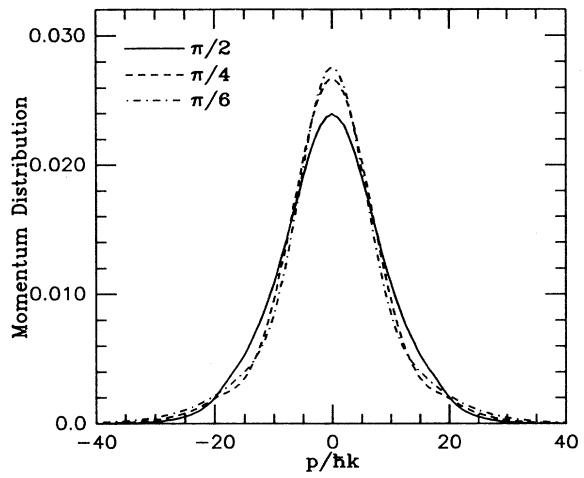

FIG. 3. Atomic momentum distribution when $J_e=\frac{1}{2}$. $U_0/E_k=500$ and $\theta=\pi/2$ (solid line), $\pi/4$ (dashed line), and $\pi/6$ (dot-dashed line).

ed. In the following, we first present the results obtained for the case of $J_e=\frac{1}{2}$. Then, as a comparison, we briefly describe the corresponding results for $J_e=\frac{3}{2}$.

Figure 2 shows the variation of the populations in the lowest six bands,

$$\Pi_\nu=\sum_q(\pi_{\nu,q,+}+\pi_{\nu,q,-}),\quad \nu=0,\ldots,5\ , \tag{24}$$

as a function of the dimensionless parameter U_0/E_k with different values of θ for $J_e=\frac{1}{2}$. As one can see from Fig. 2, when θ decreases from $\pi/2$, the population of the motional ground state Π_0, as well as the ratios between populations in the ground state and the lowest excited energy bands, i.e., Π_0/Π_ν, $\nu\geq 1$, increases for laser intensities greater than those required for achieving maximum values for Π_0. For example, Π_0 increases by more than 30% when θ is reduced from $\pi/2$ to $\pi/6$ in the laser intensity range approximately given by $U_0/E_k\geq 500$.

Such a variation of the atomic populations among different bands with θ is also evident from the atomic-momentum distribution function. Again for $J_e=\frac{1}{2}$, Fig. 3 shows the momentum distribution curves for a potential height $U_0/E_k=500$ and $\theta=\pi/2$, $\pi/4$, and $\pi/6$. One finds that as θ decreases, the width of the central peak becomes narrower, corresponding to an increase of the motional ground-state population relative to those of the lowest excited bands. On the other hand, the amplitude of the wing in the momentum distribution becomes larger as θ decreases, owing to a slight increase in the populations of some highly excited bands. The average atomic kinetic energy can be calculated as well. Figure 4 shows the variations of $\langle p^2\rangle/2m$ as a function of U_0/E_k for $\theta=\pi/2$, $\pi/4$, and $\pi/6$ for the case of $J_e=\frac{1}{2}$. As in the semiclassical results of Ref. [8], the absolute minimum

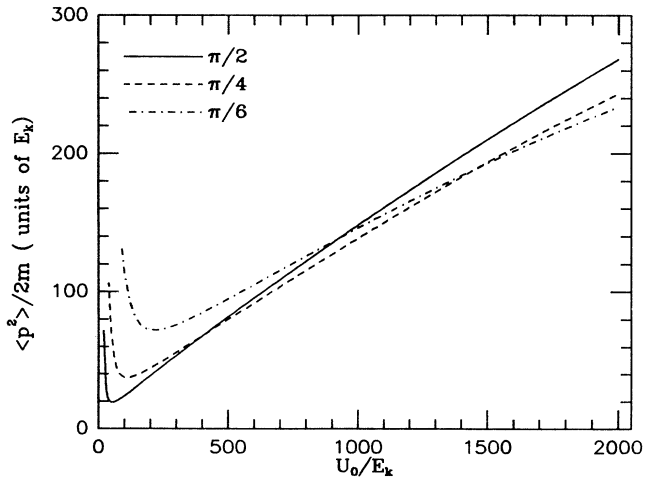

FIG. 4. Average kinetic energy of atoms as a function of U_0/E_k when $J_e=\frac{1}{2}$. $\theta=\pi/2$ (solid line), $\pi/4$ (dashed line), and $\pi/6$ (dot-dashed line).

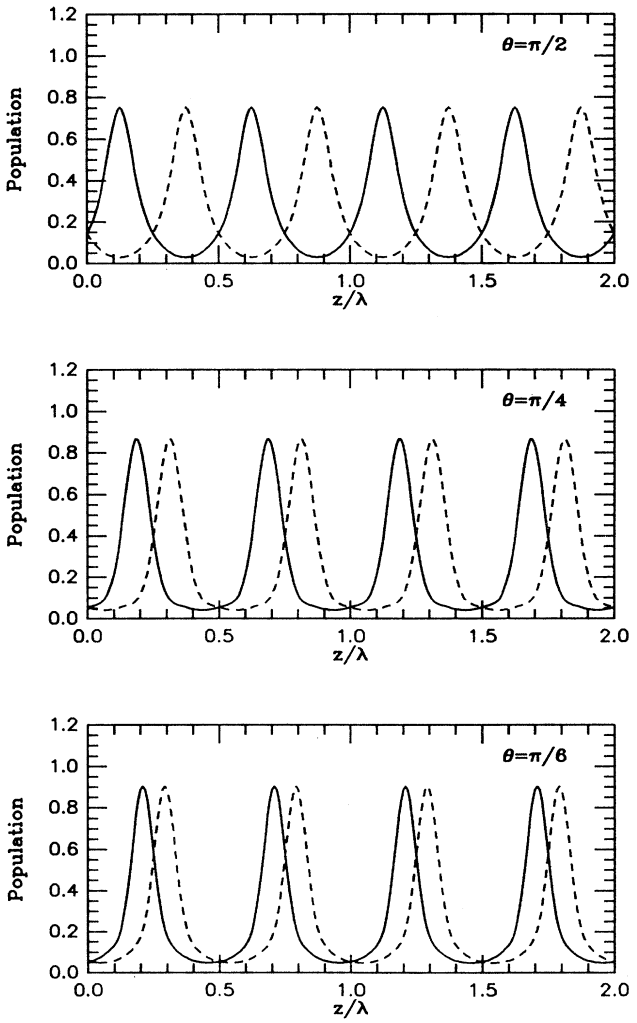

FIG. 5. Steady-state spatial distribution of the atomic population when $J_e=\frac{1}{2}$. The solid line corresponds to the internal state $|g,\frac{1}{2}\rangle$, while the dashed line corresponds to $|g,-\frac{1}{2}\rangle$. The potential height is given by $U_0/E_k=500$.

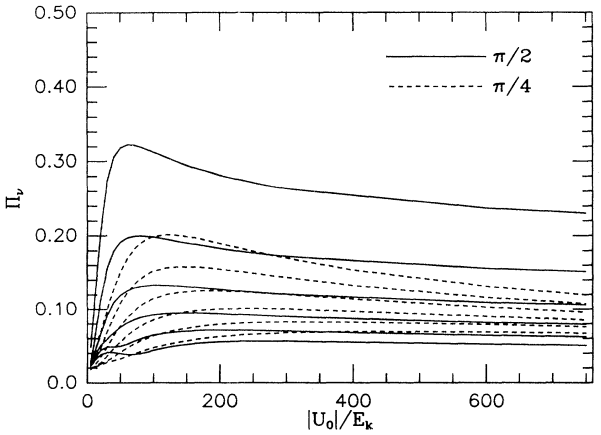

FIG. 6. Atomic populations in the lowest six motional bands as functions of $|U_0|/E_k$ when $J_e=\frac{3}{2}$. The solid line corresponds to $\theta=\pi/2$, and the dashed line to $\theta=\pi/4$.

value for the mean kinetic energy of atoms is achieved when $\theta=\pi/2$. In higher laser intensity range, however, $\langle p^2\rangle/2m$ increases more slowly with U_0/E_k for smaller angle θ, which is in qualitative agreement with the semiclassical results [8].

Finally, for $J_e=\frac{1}{2}$, we plot in Fig. 5 the steady-state spatial distribution of the atomic population in the $|g,\pm\frac{1}{2}\rangle$ ground states for three values of θ ($\pi/2$, $\pi/4$, and $\pi/6$). As expected, the atomic density is strongly modulated in space for all cases. As θ is reduced, the distance between adjacent peaks decreases as θ/k, and each population peak becomes noticeably sharper as well, owing to an increase in the motional ground-state population. When $\theta\ll 1$, there exists large local gradients in the magnetization density, owing to a change of the atomic population from the $|g,\pm 1/2\rangle$ state to the $|g,\mp 1/2\rangle$ state over a distance of θ/k.

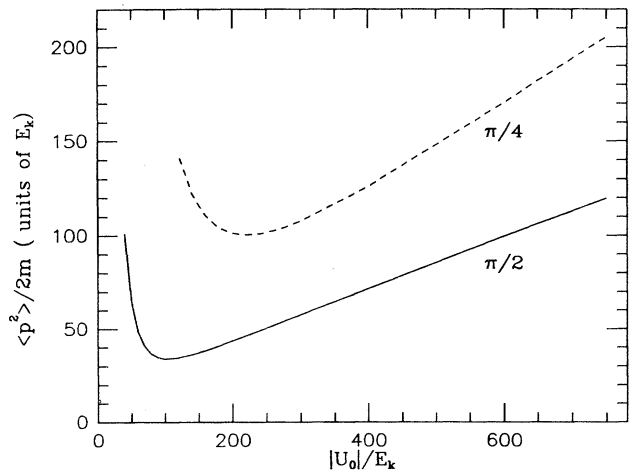

FIG. 7. Average kinetic energy of atoms as a function of $|U_0|/E_k$ when $J_e=\frac{3}{2}$. The solid line corresponds to $\theta=\pi/2$, and the dashed line to $\theta=\pi/4$.

At this point, we should point out that, although the value of θ can be chosen to be much smaller than $\pi/2$, it should remain finite in order to maintain sub-Doppler cooling. When θ goes to zero, the equilibrium value of $\langle p^2\rangle/2m$ starts to become comparable to $\hbar\Gamma$. In this case, one needs to consider the effects of Doppler cooling or heating as well, which is not included in this theory.

So far, we have described only the case of $J_e=\frac{1}{2}$. In contrast to the semiclassical calculation of Ref. [8], the results are qualitatively different for a $J_g=\frac{1}{2}\rightarrow J_e=\frac{3}{2}$ transition when effects of atomic localization are included. We plot, in Fig. 6, the populations in the lowest six bands, Π_ν, $\nu=0,\ldots,5$, as functions of $|U_0|/E_k$ for the case of $J_e=\frac{3}{2}$. As θ is reduced from $\pi/2$ to $\pi/4$, the populations in these lowest bands are significantly reduced. The average atomic kinetic energy as a function of $|U_0|/E_k$ for $J_e=\frac{3}{2}$ is shown in Fig. 7. As one can see, the value of $\langle p^2\rangle/2m$ increases faster with $|U_0|/E_k$ in the case of $\theta=\pi/4$ than $\theta=\pi/2$. Unlike in Fig. 4, the crossings between curves associated with different θ's do not occur in the case of $J_e=\frac{3}{2}$.

IV. DISCUSSION

In this section, we attempt to give some physical insight into the results of the preceding section based on the spatial localization of atoms in the light-shift potential wells. In particular, the important difference between a $J_g=\frac{1}{2}\rightarrow J_e=\frac{1}{2}$ transition and a $J_g=\frac{1}{2}\rightarrow J_e=\frac{3}{2}$ transition is addressed.

To understand the results presented above, it is helpful to first briefly review the physical mechanism in the semiclassical picture that leads to an increased cooling force for atoms with small velocities with reduced θ. As discussed in Ref. [8], there are spatial regions that correspond to the "quasinodes" of the field when $\theta\ll 1$, where the overall field intensity is very small. As a result, there is a large lengthening of the effective optical pumping time of the atomic internal states in these regions. When atoms with small velocities move across these quasinodes of the field, they can move further up the light-shift potential of one internal substate than they can in the case of lin⊥lin, and lose more kinetic energy before they are optically pumped into the potential associated with the other internal substate. Therefore, on the average, atoms with slow velocities experience stronger forces when $\theta\ll 1$ than in the case of lin⊥lin configuration.

The semiclassical argument above assumes that atoms are uniformly distributed in space. When the quantized atomic center-of-mass motion is included in the calculation, the atoms are found to be localized near the minima of the light-shift potential wells. To produce sub-Doppler cooling, the field detuning Δ is positive when $J_e=\frac{1}{2}$, and negative when $J_e=\frac{3}{2}$. The light-shift potentials for both $J_e=\frac{1}{2}$ and $\frac{3}{2}$ are shown in Fig. 8 for a small angle θ. In the case of $J_e=\frac{1}{2}$, the minima of the light-shift potential correspond to the *nodes* of the circular components of the field. Therefore, when $\theta\ll 1$, atoms

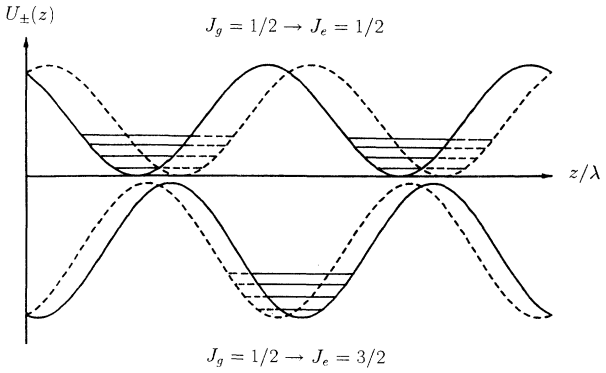

FIG. 8. Light-shift potential curves associated with each internal atomic sublevel for both $J_g = \frac{1}{2} \rightarrow J_e = \frac{1}{2}$ and $J_g = \frac{1}{2} \rightarrow J_e = \frac{3}{2}$ transitions. The solid line corresponds to $U_+(z)$, while the dashed line corresponds to $U_-(z)$. The localizations of the lowest motional bands near the potential minima are represented by the horizontal solid ($|g, \frac{1}{2}\rangle$) and dashed ($|g, -\frac{1}{2}\rangle$) lines.

in the lowest motional bands, which correspond to atoms with slow velocities in the semiclassical picture, are localized near the quasinodes of the overall field. As a result, atoms in these lowest bands experience a stronger cooling than in the case of lin⊥lin, which leads to an increase in the population of the motional ground state as θ decreases from $\pi/2$, as is evident from Fig. 2.

On the other hand, the situation is different for $J_e = \frac{3}{2}$. Since Δ is negative, the minima of the light-shift potential now correspond to the *antinodes* of the circular components of the field. As a result, the strong cooling mechanism originating from atoms moving across the quasinodes of the field is lost when the atomic spatial localization is taken into account. Moreover, atoms localized near the antinodes of the field experience a stronger diffusion due to the increased number of absorption-spontaneous emission processes. This explains qualitatively why, on one hand, one recovers the qualitative features of the semiclassical results in the case of $J_e = \frac{1}{2}$ as regard to the average atomic kinetic energy, on the other hand, cooling is significantly reduced in the case of $J_e = \frac{3}{2}$ as θ decreases from $\pi/2$ [12].

It may be possible to experimentally observe some of the features predicted by this theory for the case of $J_e = \frac{1}{2}$, with an $F \rightarrow F$ hyperfine transition. For example, in the experiment of Ref. [2], where the fluorescence spectrum of atoms confined in 1D molasses is collected, the ratio between the areas of the two Raman sidebands is believed to be proportional to the ratio between the populations in the motional ground and excited bands. Therefore an increase in the population of the motional ground state when θ is reduced should be observable through this type of technique.

The change in the spatial atomic distribution as θ is varied [see Fig. 5] may be monitored as well by a probe absorption experiment similar to the one described in Ref. [1], where a sharp dispersive line shape in the probe absorption spectrum, centered at zero pump-probe detuning, is attributed to the interference between the probe field, and the backscattered pump field from the atomic population grating. The pump field components backscattered at different spatial locations can add up constructively due to an exact compensation between the propagation phase of the field and the extra phase introduced from the scattering processes [1]. In the case of $\theta \ll \pi/2$, however, such an exact compensation of phase disappears, and one therefore expects a significant decrease in the magnitude of the central Rayleigh structure as θ is reduced, while the Raman sidebands remain unchanged or even increased in magnitude.

Finally, we would like to comment on a possible generalization of this lin∠lin scheme to a transient regime. As shown in Fig. 5, the atoms in steady state are localized around the spatial regions of either σ^+ or σ^- field polarizations, and the distance between these regions can be modulated through a variation of the angle θ between the cooling field polarization vectors. In a transient situation, one can oscillate the angle θ around some average value. For example, one can fix the polarization of one field along the x axis, while oscillate that of the counterpropagating field around y axis at some frequency δ. This leads to a situation similar to the crystal lattice oscillation in solids, with an oscillation frequency δ. If the amplitude of the oscillation angle θ_0 is sufficiently small, the effects introduced by this oscillation of the polarization vector can be treated as a perturbation. In fact, one can show explicitly that, to lowest order in θ_0, such a perturbation is equivalent to fixing the polarization of this cooling field at the y direction, while adding a pair of copropagating "probe" fields of frequencies $\omega \pm \delta$, respectively, with their polarizations perpendicular to the y axis. If the polarization oscillation frequency δ is equal to that of the atomic motion in the potential wells, i.e., Ω_{osc}, one should expect to see resonant transitions of atoms between lower and higher bands through stimulated Raman processes [1]. The effects related to these transitions may be observable through spectroscopy of these cooled atoms.

In summary, we have presented a calculation for the steady-state atomic density matrix in a 1D laser-cooling scheme, where the field consists of a pair of linearly polarized fields, with their polarizations at an angle θ to each other. The quantized atomic motion in the light-induced potentials is included in our calculation. The atomic population distribution associated with each ground-state internal sublevel is modulated in space. The distance between the population distribution peaks that correspond to the $|g, \frac{1}{2}\rangle$ and $|g, -\frac{1}{2}\rangle$ sublevels can be controlled through variation of the angle θ. As θ is reduced from $\pi/2$, the atomic population in the motional ground state increases in the case of a $J_g = \frac{1}{2} \rightarrow J_e = \frac{1}{2}$ transition, while it decreases in the case of a $J_g = \frac{1}{2} \rightarrow J_e = \frac{3}{2}$ transition, in certain laser intensity range. For $J_e = \frac{1}{2}$, the average kinetic energy of atoms increases more slowly with the laser intensity for smaller angle θ, which is in qualitative agreement with the prediction of a

semiclassical calculation. This is not the case, however, for $J_e = \frac{3}{2}$, where $\langle p^2 \rangle / 2m$ increases faster with laser intensity for smaller θ. Such a difference is directly related to the spatial localization effects of atoms in the light-shift potential wells.

ACKNOWLEDGMENTS

This research is supported by the U.S. Office of Naval Research and the National Science Foundation through Grants Nos. PHY9113590 and INT8815036.

*Present address: JILA, University of Colorado, Boulder, CO 80309-0440.

†Permanent address: Physics Department, University of Michigan, Ann Arbor, MI 48109.

[1] P. Verkerk, B. Lounis, C. Salomon, C. Cohen-Tannoudji, J.-Y. Courtois, and G. Grynberg, Phys. Rev. Lett. **68**, 3861 (1992).

[2] P. Jessen, C. Gerz, P. D. Lett, W. D. Phillips, S. L. Rolston, R. J. C. Spreeuw, and C. I. Westbrook, Phys. Rev. Lett. **69**, 49 (1992).

[3] B. Lounis, P. Verkerk, J.-Y. Coutois, C. Salomon, and G. Grynberg, Europhys. Lett. **21**, 13 (1993).

[4] P. Marte, R. Dum, R. Tâieb, and P. Zoller, Phys. Rev. A **47**, 1378 (1993).

[5] Y. Castin, J. Dalibard, and C. Cohen-Tannoudji, in *Light Induced Kinetic Effects of Atoms and Molecules,* edited by L. Moi *et al.* (Ets Editrice, Pisa, 1990); O. Emile *et al.*, to be published in J. Phys. (France) II.

[6] R. Dum, P. Zoller, and H. Ritsch, Phys. Rev. A **45**, 4879 (1992).

[7] J. Dalibard, Y. Castin, and K. Mølmer, Phys. Rev. Lett. **68**, 580 (1992).

[8] V. Finkelstein, P. R. Berman, and J. Guo, Phys. Rev. A **45**, 1829 (1992).

[9] Y. Castin and J. Dalibard, Europhys. Lett. **14**, 761 (1991).

[10] Y. Castin, H. Wallis, and J. Dalibard, J. Opt. Soc. Am. B **6**, 2046 (1989).

[11] M. Wilkens, E. Schumacher, and P. Meystre, Phys. Rev. A **44**, 3130 (1991).

[12] R. Tâieb, P. Marte, R. Dum, and P. Zoller, Phys. Rev. A **47**, 4986 (1993).